

A process-based approach to estimate point snow instability

Benjamin Reuter, Jürg Schweizer, Alec van Herwijnen

WSL Institute for Snow and Avalanche Research SLF, Flüelastrasse 11, 7260 Davos Dorf, Switzerland

1 **Abstract:** Snow instability data provide information about the mechanical state of the snow cover
2 and are essential for forecasting snow avalanches. So far, direct observations of instability (recent
3 avalanches, shooting cracks or whumpf sounds) are complemented with field test such as the
4 rutschblock test, since no measurement method for instability exists. We propose a new approach
5 based on snow mechanical properties derived from the snow micro-penetrometer that takes into
6 account the two essential processes during dry-snow avalanche release: failure initiation and crack
7 propagation. To estimate the propensity of failure initiation we define a stress-based failure
8 criterion, whereas the propensity of crack propagation is described by the critical cut length as
9 obtained with a propagation saw test. The input parameters include layer thickness, snow density,
10 effective elastic modulus, strength and specific fracture energy of the weak layer – all derived from
11 the penetration-force signal acquired with the snow micro-penetrometer. Both instability measures
12 were validated with independent field data and correlated well with results from field tests.
13 Comparisons with observed signs of instability clearly indicated that a snowpack is only prone to
14 avalanche if the two separate conditions for failure initiation and crack propagation are fulfilled. To
15 our knowledge, this is the first time that an objective method for estimating snow instability has
16 been proposed. The approach can either be used directly based on field measurements with the
17 snow micro-penetrometer, or be implemented in numerical snow cover models. With an objective
18 measure of instability at hand, the problem of spatial variations of instability and its causes can now
19 be tackled.

20 1 Introduction

21 Snow slope stability describes the mechanical state of the snow cover on an inclined slope and is
22 inversely related to the probability of avalanche release (McClung and Schaerer, 2006). For a given
23 time, depth within the snowpack, and location on a slope, snow stability can be described as the
24 balance between snow strength and stress termed stability index (Roch, 1966). This index has been
25 widely used (e.g. Conway and Abrahamson, 1984; Perla et al., 1982) and refined by taking into
26 account triggering by an additional load such as a skier (Föhn, 1987). Whereas, the skier stability
27 index has been shown to be related to the probability of skier triggering (Jamieson, 1995), this critical
28 stress approach does not take into account that slope failure requires crack propagation. While
29 failure initiation may depend on stress only, the propagation of cracks requires deformation energy
30 (Bazant and Planas, 1998). Furthermore, on a slope, strength and stress are spatially variable; these
31 variations are fundamental to the fracture process (Schweizer et al., 2003). Around locally failed
32 areas stress concentrations will form and drive crack propagation, and eventually cause catastrophic
33 failure before the average material strength is reached. This observation has been termed knock-
34 down effect (Fyffe and Zaiser, 2004) and partly explains why the stability index derived from
35 measurements at or near natural slab avalanches often indicated stable conditions (Perla, 1977).

36 Not surprisingly, the link between point observations of snow stability and snow slope stability is not
37 clear, yet (e.g. Bellaire and Schweizer, 2011). Scale issues due to different measurement scales, the
38 so-called support and knowledge gaps between the processes involved at both scales have
39 complicated bringing together point and slope scale snow instability results (Schweizer et al., 2008a).
40 The point stability scale is not even well defined. Failure initiation refers to the collective failing of
41 snow grains, or bonds between grains, on the scale of centimeters and the onset of a self-
42 propagating crack in a weak snow layer called crack propagation. A common scale for both processes
43 is the snowpack scale which spans about one square meter (Schweizer and Kronholm, 2007) which in
44 the following we will refer to when we use the term point snow instability.

45 The stability index assumes a transition from stable to unstable when driving forces are no longer
46 balanced by resisting forces. However, this approach is questionable, primarily since dry-snow slab
47 avalanche release is the result of a series of fractures and snow properties are spatially variable. In a
48 fracture mechanical view, to describe a material's resistance to crack propagation, flaw size and
49 toughness need to be considered additionally to the stresses (Anderson, 1995). With the
50 introduction of the propagation saw test (PST) (Gauthier and Jamieson, 2006; Sigrist and Schweizer,
51 2007) all these properties can be obtained from field data. PST experiments to study propagating
52 cracks have confirmed deformation of the slab to substantially contribute to the mechanical energy
53 consumed by crack extension (van Herwijnen et al., 2010). Further, Gauthier and Jamieson (2008b)
54 have shown that the critical crack length together with the fracture result are related to slope
55 instability. In particular, cracks propagating to the end of the column after saw cut lengths less than
56 50 % of the column length were clear indicators of high crack propagation propensity.

57 There is presently no objective measurement of snow instability. Instead, recent avalanches,
58 whumpfs or shooting cracks are considered indicators of instability (Jamieson et al., 2009), but these
59 observations are rare. In their absence the remaining option to gather field data on snow instability is
60 snow instability testing (Schweizer and Jamieson, 2010). The rutschblock (RB) is a traditional snow
61 stability test (Schweizer, 2002). The RB score was found indicative of the failure initiation propensity,
62 the RB release type of the crack propagation propensity (Schweizer et al., 2008b). Whereas the RB
63 release type only represents an ordinal rank, the propagation saw test (PST) gives a metric value, the
64 critical cut length, which eases quantitative analysis. A combination of the results of both tests
65 therefore seems appropriate for snow instability assessment.

66 Several studies focused on snow instability in the past, thereby either concentrating on failure
67 initiation or crack propagation. Both, Bellaire et al. (2009) and Pielmeier and Marshall (2009) derived
68 stability related parameters from measured snow micro-penrometer resistance profiles. They
69 found that weak layer strength and average slab density predicted with good accuracy stability
70 classes estimated from RB tests.

71 Under the assumption of a uniform slab on a rigid substratum Heierli (2008) presented estimates of
72 critical crack lengths obtained from recalculation of PST field experiments. Yet, averaging slab
73 properties is a strong simplification and Schweizer (1993) pointed out the importance of slab
74 properties for failure initiation. By means of linear elastic finite element (FE) simulations of typical
75 snow profile types Habermann et al. (2008) found the stress at the depth of the weak layer to vary by
76 a factor of two compared to a uniform slab. McClung (2009) suggested an alternative model to
77 estimate the critical crack length by considering a finite fracture process zone.

78 Several numerical approaches focusing on avalanche release (for a summary see Podolskiy et al.,
79 2013) have been made but only a few incorporate both fracture processes. Among the latest were
80 Gaume et al. (2013) who presented a Mohr-Coulomb failure criterion based model taking into
81 account variations of weak layer shear strength and stress redistribution by slab elasticity. Only
82 lately, a possible refinement of the classical stability index by accounting for strength variations and
83 their knock-down effect including a derivation of a critical crack length was presented (Gaume et al.,
84 2014).

85 Predicting snow instability requires snow properties obtained either from field measurements or
86 from snow cover modeling. In the field, the method of choice is the snow micro-penetrometer (SMP)
87 (Schneebeli and Johnson, 1998) that allows deriving microstructural and micromechanical properties
88 from the penetration force-distance signal (Johnson and Schneebeli, 1999). Marshall and Johnson
89 (2009) showed that values of snow density, elastic modulus and strength derived from snow micro-
90 penetrometer signals compared well with literature data. Interpreting the oscillation of the
91 penetration force as a Poisson shot-noise process Löwe and van Herwijnen (2012) suggested a more
92 robust method to extract the microstructural parameters. Their method was employed by Proksch et
93 al. (2014) who developed a reliable parameterization of snow density applicable to a wide range of
94 snow types. Reuter et al. (2013) showed that with the snow micro-penetrometer apart from snow
95 density and effective modulus also the specific fracture energy of the weak layer can be derived.
96 Comparing the results for mechanical properties obtained with snow micro-tomography (Schneebeli,
97 2004) to those with particle tracking velocimetry of propagation saw tests (van Herwijnen et al.,
98 2010) they substantiated the reliability of SMP-derived parameters.

99 Alternatively, snow cover models provide snow structural information allowing snow instability
100 modeling (Durand et al., 1999; Lehning et al., 2004). However, snow mechanical properties are often
101 not simulated independently, but parameterized on density only. Schweizer et al. (2006) refined the
102 skier's stability index implemented in the snow cover model SNOWPACK and validated it with field
103 observations. By first identifying the potential weakness in a simulated profile and then assessing its
104 stability Monti et al. (2014) improved this approach to classify profiles into three classes of snow
105 instability: poor, fair and good.

106 Given the fracture mechanical context of dry-snow slab avalanche release and the lack of an
107 objective measure of instability, we propose that a description of instability should take into account
108 the two essential processes in slab avalanche release, i.e. failure initiation and crack propagation,
109 and be based on snow mechanical properties measured with the snow micro-penetrometer. Our goal
110 is to provide an observer-independent methodology applicable to field measurements of snow
111 stratigraphy. To this end we introduce a two-step calculation of a stability criterion and a critical
112 crack length based on snow mechanical properties measured with the SMP. Then, we will validate
113 the performance of our approach with field experiments of snow instability. Finally, we will show
114 how classical snow instability observations may be interpreted in terms of failure initiation and crack
115 propagation.

116 **2 Methods**

117 First, we present the experimental data, and then we describe how the mechanical field data
118 acquired with the snow micro-penetrometer was analyzed, before we introduce the new approach
119 to derive snow instability.

120 2.1 Field data

121 Two datasets of SMP measurements were exploited to test the performance of the failure initiation
122 (A) and the crack propagation (B) part of our approach. Dataset A was originally presented by Bellaire
123 et al. (2009). As meta data on snow instability was only available for a share of the data, 64 SMP
124 measurements were kept for further analysis. They were all performed in close proximity (<0.5 m) to
125 a RB test. The main results of a RB test, which is a point observation, are score and release type
126 (Figure 1). We used the score for validating the failure initiation propensity (Schweizer and Jamieson,
127 2010).

128 Dataset B consists of 31 SMP measurements which have been performed in a distance less than
129 30 cm from the lower end of the column of propagation saw tests (PST) (Figure 2). Data were
130 collected on seven different days. We filmed the fractures in the PSTs to precisely determine the
131 onset of propagation by measuring the critical cut length in the pictures as a criterion of crack
132 propagation.

133 Both datasets also include manually observed snow profiles including snow grain type and size and
134 hand hardness index for each manually identified layer. In addition, 77 out of the 95 field records in
135 total contain information on either type or absence of signs of instability.

136 2.2 Snow micro-penetrometer

137 With the snow micro-penetrometer (SMP) a penetration resistance profile is recorded to a depth
138 well below the weak layer at sub-millimeter resolution. Based on the detailed manually observed
139 snow profile layers were defined from the corresponding sections of the signal, namely slab layers, a
140 weak layer and a basal layer. As every layer is later represented in a finite element (FE) model and
141 the resolution of the SMP is higher than the one needed for FE simulations, we deal with layers for
142 the sake of shorter computation times. Figure 3 shows an example of a SMP signal with manually
143 assigned snow layer boundaries.

144 Applying the shot-noise model by Löwe and van Herwijnen (2012) snow micro-structural parameters,
145 namely the rupture force f , the deflection at rupture δ and the structural element size L were
146 calculated over a moving window w of 2.5 mm with 50% overlap and then averaged over the layer.
147 Snow density was calculated as described in Proksch et al. (2015):

$$148 \quad \rho = a_1 + a_2 \log(\tilde{F}) + a_3 L \log(\tilde{F}) + a_4 L \quad (1)$$

149 where a_i are coefficients, F is the penetration resistance and tilde denotes the median. The micro-
150 mechanical effective modulus and strength were calculated according to Johnson and Schneebeli
151 (1999):

$$152 \quad E = \frac{f}{\delta L} \quad (2)$$

153 and

$$154 \quad \sigma = \frac{f}{L^2} \quad (3)$$

155 The specific fracture energy of the weak layer (WL) was calculated as the minimum of the
156 penetration resistance integrated across the window size w within the weak layer (Reuter et al.,
157 2013):

158 $w_f = \min_{WL} \int_{-\frac{w}{2}}^{+\frac{w}{2}} F dz .$ (4)

159 The penetration depth PS was calculated from Eq. 5 by integrating the penetration resistance F from
 160 the snow surface to PS until a threshold absorbed energy $e_a= 0.036$ J is reached. The value of e_a has
 161 been determined by comparison of SMP profiles with concurrently observed penetration depth
 162 (Schweizer and Reuter, 2015):

163 $e_a = \int_0^{PS} F(z) dz.$ (5)

164 **2.3 Modeling**

165 In the following the modeling approach to calculate estimates of the failure initiation and the crack
 166 propagation propensity of a certain slab-weak layer combination is described and validated. The
 167 mechanical properties required as input are obtained from the SMP signal as described above.

168 *2.3.1 Failure initiation*

169 A strength-over-stress criterion S describes the propensity of the weak layer to fail in the case of an
 170 additional load:

171 $S = \frac{\sigma_{WL}}{\Delta\tau},$ (6)

172 with σ_{WL} being the strength of the weak layer and $\Delta\tau$ being the maximum additional shear stress at
 173 the depth of the weak layer due to skier loading. The strength of the weak layer is approximated by
 174 the micro-mechanical strength derived from the snow micro-penetrometer signal in the weak layer,
 175 i.e. we cannot use the slope-parallel shear strength because the SMP is an indentation test
 176 measuring an effective strength resulting from the mixed-mode breaking of bonds at the tip. The
 177 maximum shear stress at the depth of the weak layer was modeled with the 2D linear elastic finite
 178 element (FE) model originally designed by Habermann et al. (2008) to calculate the shear stress at
 179 the depth of the weak layer below a layered slab due to the weight of a skier. S may be interpreted
 180 as an indicator of failure initiation with low (high) values being associated with high (low) likelihood
 181 of initiating a failure. Note, the stability criterion S is not expected to yield typical values of the skier's
 182 stability index (< 1 for 'unstable', > 1.5 for 'stable') (Jamieson and Johnston, 1998). One reason is that
 183 SMP-derived strength values are about two orders of magnitude larger than values of shear strength
 184 reported in literature (Marshall and Johnson, 2009). As the SMP is a small scale indentation test, the
 185 difference between strength values measured with the SMP and the shear frame test (Jamieson and
 186 Johnston, 2001) may be attributed to sample size and type of loading.

187 The 2D FE model by Habermann et al. (2008) has been adopted to include all relevant slab layers –
 188 usually about 5 to 10 layers. The geometry of the model (Figure 4a) was chosen such that the length
 189 of the modeled section of the snowpack (10 m) is at least one order of magnitude larger than the
 190 average depth of the weak layer to keep boundary effects small. The model consists of multiple
 191 layers including slab and basal layers as well as an embedded weak layer corresponding to the
 192 layering identified in the SMP signal. The layers are inclined by the slope angle α . Nodes at the lower
 193 end (on the right of Figure 4a) and at the snow soil interface were fixed in both coordinate directions.

194 The model domain was divided into two-dimensional, quadrilateral plane strain elements having
 195 eight nodes each. The mesh consisted of 75 nodes in the horizontal and 100 nodes in the vertical per
 196 meter. The model has been implemented in ANSYS workbench to calculate the maximum shear
 197 stress within the weak layer. We assumed plane strain as stresses in the direction normal to the x-y
 198 plane are smaller than within and linear elastic behavior as the loading rate is high considering skier
 199 loading. The skier load was modeled as a static strip load P of 780 N spread over a width a of 0.2 m.
 200 To account for skier penetration we assumed the layers within the penetration depth to be
 201 compacted to a density of 300 kg m^{-3} with a corresponding elastic modulus of 16 MPa according to
 202 Scapoza (2004); the thickness of those slab layers was adjusted so that the mass remained the
 203 same. All snow layers in the FE model were assigned thickness, density and effective modulus values
 204 as derived from the SMP signal. A fixed value of the Poisson's ratio was chosen ($\nu = 0.25$), as its
 205 influence is small compared to our measurement uncertainties for density or elastic modulus. From
 206 the modeled linear elastic behavior the maximum shear stress within the weak layer was computed
 207 yielding $\Delta\tau$ of Eq. 6, i.e. not considering the stress due to the weight of the slab.

208 The FE model was tested to reproduce the analytical solution of McClung and Schweizer (1999) for
 209 the shear stress for a strip load on a finite area $\tau(\theta, H)$ where θ and H are two-dimensional polar
 210 coordinates. To do so, the maximum shear stress at a certain depth H was determined by varying θ .
 211 The FE model was run with a Poisson's ratio of $\nu = 0.49$, as the analytical solution assumes an
 212 incompressible half space. The slab was not stratified, but uniform having a density of 200 kg m^{-3} .
 213 Hence, the solution is independent of the elastic modulus. The simulation results for different slab
 214 thickness H are presented in Figure 4b together with the analytical solution. The FE model
 215 reproduced the maximum shear stress as obtained with the analytical solution very well ($R^2 = 0.94$,
 216 regression slope $m = 1.2$) especially for slab depth larger than the width of skier load (0.2 m).

217 2.3.2 Crack propagation

218 In order to estimate the crack propagation propensity the critical crack length as measured in a PST
 219 experiment was calculated for a weak layer embedded by a layered slab and a basal layer.

220 A theoretical expression (Eq. 7) linking the fracture energy of the weak layer, the elastic modulus of
 221 the slab and the critical crack length for a self-propagating crack is obtained by replacing the
 222 mechanical energy in Griffith's criterion with the total energy of the slab weak layer system found by
 223 Heierli (2008) and was presented in detail by Schweizer et al. (2011). The formulation of the total
 224 mechanical energy of the slab-weak layer system has been proven to describe the released
 225 mechanical energy of the slab in a PST reasonably well (van Herwijnen et al., 2010).

$$226 \quad w_f(E, r_c) = \frac{H}{2E} \left[w_0 + w_1 \frac{r_c}{H} + w_2 \left(\frac{r_c}{H} \right)^2 + w_3 \left(\frac{r_c}{H} \right)^3 + w_4 \left(\frac{r_c}{H} \right)^4 \right], \quad (7)$$

227 with

$$w_0 = \frac{3\eta^2}{4} \tau^2,$$

$$w_1 = \left(\pi\gamma + \frac{3\eta}{2} \right) \tau^2 + 3\eta^2 \tau\sigma + \pi\gamma\sigma^2,$$

$$w_2 = \tau^2 + \frac{9\eta}{2} \tau\sigma + 3\eta^2 \sigma^2,$$

$$w_3 = 3\eta\sigma^2,$$

$$w_4 = 3\sigma^2,$$

228 and $\tau = -\rho g H \sin(\alpha)$ the shear stress, $\sigma = -\rho g H \cos(\alpha)$ the normal stress, γ the elastic mismatch
 229 parameter, which is about one according to Heierli (2008), $\eta = \sqrt{4(1 + \nu)/5}$ and $\nu = 0.25$. Provided
 230 the elastic modulus E , the density ρ and the thickness of the slab H , the fracture energy of the weak
 231 layer w_f , and the slope angle α are known, the calculation of the critical crack length r_c reduces to
 232 finding the roots of Eq. 7. This fourth degree polynomial of r_c has real, ever positive coefficients.
 233 Figure 5 illustrates the dependence of the polynomial's discriminant on slab thickness and density,
 234 which is the case if a dependence of the elastic modulus on density is assumed. As the polynomial's
 235 discriminant does not change sign for typical values of density (and the elastic modulus), solutions
 236 consist of a pair of complex conjugated and two real roots. A physically meaningful solution of r_c is
 237 obtained, if the complex roots and the one with an unexpected sign are discarded.

238 To relax the assumption of a uniform, i.e. not stratified, slab a FE model was designed to determine
 239 the equivalent bulk modulus E' of a stratified slab (Figure 6a). The model performed a stepwise
 240 calculation of the mechanical strain energy M of a stratified slab due to bending over an increasing
 241 crack of length r . In order to recover an equivalent bulk modulus E' , in a next step the pairs of
 242 mechanical energy and crack length (M, r) were fitted with a theoretical expression of the total
 243 mechanical energy of the slab M (Heierli, 2008):

$$244 \quad M(E', r) = -\frac{\pi \gamma r^2}{4E'} (\tau^2 + \sigma^2) - \frac{r^3}{6E'H} [\lambda_{\tau\tau} \tau^2 + \lambda_{\sigma\tau} \tau\sigma + \lambda_{\sigma\sigma} \sigma^2], \quad (8)$$

245 with

$$246 \quad \lambda_{\tau\tau} = 1 + \frac{9}{4}\eta \left(\frac{r}{H}\right)^{-1} + \frac{9}{4}\eta^2 \left(\frac{r}{H}\right)^{-2},$$

$$247 \quad \lambda_{\tau\sigma} = \frac{9}{2}\eta + \frac{9}{2}\eta^2 \left(\frac{r}{H}\right)^{-1},$$

$$248 \quad \lambda_{\sigma\sigma} = 3\eta^2 + \frac{9}{4}\eta \frac{r}{H} + \frac{9}{5} \left(\frac{r}{H}\right)^2.$$

249 The FE model consists of stratified layers, which were assigned SMP-derived values of density,
 250 effective modulus and thickness (Figure 6a). The Poisson's ratio was kept constant ($\nu = 0.25$). Due to
 251 its geometry (only considering slab layers) and boundary conditions (rigid support along the ligament
 252 length $(L-r)$) the FE model only considers the behavior of the slab layers as described with the
 253 formulation of the total mechanical energy of the slab-weak layer system, neglecting deformation in
 254 the weak or basal layers. In our model, the deflecting beam never got in touch with the basal layer,
 255 which, however, may be the case in field experiments, in particular with soft slabs. The FE model
 256 reproduced the theoretical formulation very well ($R^2 = 0.85$), especially for crack lengths r greater or
 257 equal the thickness of the overlying slab H (Figure 6b). With the bulk equivalent modulus E' , we find
 258 the exact solution of Eq. 7 and obtain the critical crack length r_c for the specific slab-weak layer
 259 combination.

260 **3 Results**

261 In the following both model parts predicting the propensity of the snowpack to failure initiation and
 262 crack propagation are evaluated with the two independent data sets (A and B).

263 **3.1 Failure initiation**

264 For each of the 66 SMP profiles with corresponding RB test (dataset A) the failure initiation criterion
265 S was calculated. SMP-derived density, effective modulus, strength and layer thickness were used to
266 drive the FE model. For the comparison with the RB score we grouped scores 1 and 2 as well as 6 and
267 7 because scores 1 and 7 were observed infrequently. The criterion S increased with increasing RB
268 score (Figure 7a). If for a given S there was no overlap of the boxes, the predictive power of S would
269 obviously be very good. Although this is not the case, the medians of the failure initiation criterion
270 (indicated by gray lines) per RB score increased monotonically with increasing RB scores. This
271 monotonic increase is reflected in a high Spearman rank correlation coefficient ($r_s > 0.9$). If results are
272 grouped by scores in two stability classes of $RB < 4$ and $RB \geq 4$, a threshold previously found to
273 separate lower and higher stability (e.g. Schweizer and Jamieson, 2003), the criterion S discriminated
274 well between the two classes (Wilcoxon rank sum test, level of significance $p = 0.01$) with a
275 classification tree splitting value of $S = 133$.

276 **3.2 Crack propagation**

277 All 31 SMP signals from dataset B were analyzed and the critical cut length r_c was calculated from
278 Eq. 7 with SMP-derived mechanical properties being density, effective modulus, specific fracture
279 energy and layer thickness. In Figure 8 the results are contrasted with the critical crack lengths
280 measured in the field in the PST experiments adjacent to the SMP measurements. On the left
281 (Figure 8a) model results are shown for the case of a uniform slab, i.e. density and effective modulus
282 were averaged to show the effect of neglecting the stratigraphy of the slab. Modeled values
283 overestimated the critical cut length yielding a rather fair Pearson correlation coefficient of $r_p = 0.58$
284 and a coefficient of determination of $R^2 = 0.29$. Only for a few experiments modeled and observed
285 crack lengths were similar indicating that assuming a uniform slab is not a good approximation. In
286 fact, Figure 8b shows that the agreement between model results and observations improved if the
287 stratification of the slab was taken into account. All identified slab layers were assigned the
288 corresponding density and effective modulus obtained from SMP signal processing and input in the
289 FE model to determine the bulk effective modulus of the slab. The modeled values of critical crack
290 length were clearly related to the measured values ($r_p = 0.83$) as indicated by the collapse of the
291 linear regression on the 1:1 line (Figure 8b). The regression slope was well-defined ($p < 0.01$) with
292 some scatter ($R^2 = 0.50$) indicating the uncertainty involved with the presented approach. The critical
293 crack length was predicted with a root mean squared error of 2 cm, a mean absolute error of 7 cm
294 and a mean absolute percentage error of 9%.

295 **3.3 Validation with signs of instability**

296 Model results were further compared with independent field observations of signs of instability such
297 as whumpfs, shooting cracks and recent avalanches. Both datasets (A and B) included records of such
298 field observations which we grouped in three categories: whumpfs, shooting cracks with or without
299 whumpfs ('cracks') or 'all signs' (whumpfs, cracks and recent avalanches), i.e. fresh avalanches were
300 only observed simultaneously with whumpfs and cracks (Figure 9). To jointly relate our modeled
301 estimates of instability to the observations of instability we contrasted the propensity to crack
302 propagation, i.e. modeled critical crack length, and failure initiation, i.e. initiation criterion S , in
303 Figure 9. Signs of instability were primarily present in the lower left of Figure 9, i.e. for low values of
304 the failure initiation criterion and the critical crack length. Vice versa no signs of instability were

305 reported if both criteria yielded high values (upper right). This finding suggests that both criteria, the
306 one for failure initiation and the one for crack propagation, are linked to snow instability. A
307 classification tree with the two independent variables S and r_c yielded splits of $S = 234$ and $r_c = 0.41$ m
308 which separate between the cases with and without concurrently observed signs of instability (Figure
309 9). These thresholds divide the plot into four quadrants. In the lower left quadrant all 35 cases with
310 signs of instability as well as ten cases without signs of instability were found. Our split value ($S=234$)
311 for the initiation criterion S is very similar to the one found by Schweizer and Reuter (2015) who
312 reported a value of 212. In regard to the modeled critical crack length, Gauthier and Jamieson
313 (2008a) suggested a value of <50% of the column length which in their study corresponded to 50 cm.
314 Assuming crack propagation to be likely (two lower quadrants) or failure initiation to be easy (two
315 left quadrants) does not distinguish sharply between signs of instability present or absent. However,
316 if both criteria had low values unstable snow conditions were observed (lower left quadrant).

317 **4 Discussion**

318 In our present understanding avalanche release is seen as a sequence of fractures. To capture the
319 two most important steps preceding the detachment of a snow slab we addressed the stress at the
320 depth of a potential weakness with the failure initiation criterion S and the critical crack size for self-
321 propagation with the critical crack length r_c . We presented a model approach to derive both
322 quantities from snow micro-penetrometer signals which is a fast method to acquire information on
323 mechanical properties in the field.

324 Assessing the performance of the model approach with two different field tests (RB and PST) yielded
325 plausible results. However, the main source of uncertainty is related to the mechanical properties
326 needed as input for the model. Snow density, effective modulus and specific fracture energy were all
327 determined from SMP measurements. Uncertainties related to the determination of these
328 mechanical properties have recently been addressed by Proksch et al. (2015) and Reuter et al. (2013)
329 and lie within 10-20% for density and fracture energy. Other SMP error sources are known and so
330 erroneous signals were identified and discarded. Some errors were user-related such as mechanical
331 disturbances. Other unavoidable errors such as signal drift due to strong temperature changes in the
332 snowpack or stick slip of the rod at high snow densities were rare.

333 The SMP-derived failure initiation criterion S performed well based on the evaluation with
334 rutschblock tests, yielding a better correlation than the one lately observed by Schweizer and Reuter
335 (2014) using the compression test. They concluded that the dimensions of the compression test and
336 the type of loading are not ideal for modeling purposes. While the RB test includes six different
337 loading steps, the load is only increased twice in a compression test, but numerous taps are
338 performed within the same loading range. The loading of the RB and consequently the stress exerted
339 on the weak layer increases monotonically with the score (score four and five have the same load).
340 This is reflected in the fair discrimination of RB scores four and five with the failure initiation
341 criterion S . Furthermore, RB loading steps are ordinal numbers, i.e. they can be ranked, but they do
342 not follow a known relation with stability. Hence, the stress in the weak layer increases stepwise in
343 the experiment, whereas the modeled stability is continuous. The boxplots in Figure 7 group
344 modeled values of failure initiation (S) with rutschblock classes. The monotonic increase of the
345 medians suggests that the criterion S reflects the propensity of failure initiation in a weak layer below

346 a layered slab. Correlations of the rutschblock release type were neither significant with the initiation
347 criterion S ($r_s = 0.11$, $p = 0.39$), nor with the modeled critical cut length ($r_s = 0.04$, $p = 0.76$).

348 The critical cut length was modeled with an accuracy of a few centimeters (RMSE of 2 cm). It was
349 shown that the slab layering played an important role in the process of crack propagation. Only with
350 the introduction of the bulk effective modulus imitating the bending behavior of a layered slab
351 measured critical cut lengths were reproduced with good accuracy (Figure 8). Until now research on
352 snow instability had mainly focused on weak layer or average slab properties (Bellaire et al., 2009;
353 Pielmeier and Marshall, 2009). Alternatively, the critical value of the crack length could have been
354 determined by stepwise increasing the crack length in an FE model until the critical energy release
355 rate reaches the specific fracture energy of the weak layer. This approach, comparable to that of
356 Mahajan and Joshi (2008), however, was not followed due to its high computational expenses, as
357 repeated meshing for every single iteration step would be costly.

358 The introduced FE models assumed linear elastic behavior and were confined to two dimensions.
359 These assumptions are in contrast with our knowledge that snow is a porous medium consisting of a
360 non-isotropic ice/air matrix, exhibiting plastic, elastic and viscous behavior at the macro scale.
361 However, as loading rates in RB tests and PSTs are high, linear elastic assumptions are justified – for
362 the rutschblock test at least at a certain depth below the snow surface. Two dimensional modeling
363 seems sufficient, as three dimensional modeling is not advantageous due to the lack of experimental
364 orthotropic material properties at this point of time.

365 **5 Conclusions**

366 We have developed a novel approach to determine quantitative estimates of both, the failure
367 initiation and crack propagation propensity of the snowpack based on mechanical properties derived
368 from objective snow micro-penetrometer measurements. Based on the current understanding of
369 dry-snow slab avalanche release it includes the mechanical properties of all relevant layers
370 embedding the weak layer to make predictions on the propensity of initiating a failure and spreading
371 the crack in a weak layer within the snowpack. The presented approach is process-based, observer-
372 independent and relies on measurements of mechanical properties.

373 The performance of the two novel measures of instability has been assessed in comparisons with two
374 different datasets of field tests (rutschblock and propagation saw test). Both measures of instability,
375 the stress criterion S as well as the critical crack length r_c were well correlated with the results of field
376 tests. In addition, the importance of slab layering especially with respect to crack propagation has
377 been shown. The comparison of our modeled estimates of snow instability with field observations of
378 signs of instability clearly indicated that a snowpack is unstable only in case of high failure initiation
379 as well as high crack propagation propensity. Whereas we anticipated this finding, i.e. that both
380 conditions have to be fulfilled, we are not aware, to the best of our knowledge, that it has been
381 demonstrated before.

382 Recent field studies have frequently focused on identifying spatial variations of snow instability and
383 its drivers which requires an objective measure of instability – which was so far lacking. With the
384 observer-independent method we presented, taking into account both failure initiation and crack
385 propagation processes, it will become possible to resolve causes of spatial snow instability variations.

386 With respect to operational application in the context of avalanche forecasting, our approach based
387 on field measurements could be employed, provided a robust and reliable snow micro-penetrometer
388 is at hand which in addition allows remote data transfer and automatic processing, or be
389 implemented in numerical snow cover models.

390 **Acknowledgements**

391 B.R. has been supported by a grant of the Swiss National Science Foundation (200021_144392). We
392 thank numerous colleagues from SLF for help with the field work. We are grateful for the
393 constructive review comments by E. Podolskiy and B. Jamieson.

394 **References**

- 395 Anderson, T. L.: Fracture mechanics: fundamentals and applications, CRC Press, Boca Raton, U.S.A.,
396 1995.
- 397 Bazant, Z. P. and Planas, J.: Fracture and size effect in concrete and other quasibrittle materials, CRC
398 Press, Boca Raton, U.S.A., 1998.
- 399 Bellaire, S., Pielmeier, C., Schneebeili, M., and Schweizer, J.: Stability algorithm for snow micro-
400 penetrometer measurements, *J. Glaciol.*, 55, 805-813, 2009.
- 401 Bellaire, S. and Schweizer, J.: Measuring spatial variations of weak layer and slab properties with
402 regard to snow slope stability, *Cold Reg. Sci. Technol.*, 65, 234-241, 2011.
- 403 Conway, H. and Abrahamson, J.: Snow stability index, *J. Glaciol.*, 30, 321-327, 1984.
- 404 Durand, Y., Giraud, G., Brun, E., Mérindol, L., and Martin, E.: A computer-based system simulating
405 snowpack structures as a tool for regional avalanche forecasting, *J. Glaciol.*, 45, 469-484, 1999.
- 406 Föhn, P. M. B.: The stability index and various triggering mechanisms, in: Symposium at Davos 1986
407 – Avalanche Formation, Movement and Effects, IAHS Publ. 162, edited by: Salm, B. and Gubler,
408 H., International Association of Hydrological Sciences, Wallingford, Oxfordshire, UK, 1987, 195-
409 214.
- 410 Fyffe, B. and Zaiser, M.: The effects of snow variability on slab avalanche release, *Cold Reg. Sci.*
411 *Technol.*, 40, 229-242, 2004.
- 412 Gaume, J., Chambon, G., Eckert, N., and Naaim, M.: Influence of weak-layer heterogeneity on snow
413 slab avalanche release: application to the evaluation of avalanche release depths, *J. Glaciol.*,
414 59, 423-437, 2013.
- 415 Gaume, J., Schweizer, J., van Herwijnen, A., Chambon, G., Reuter, B., Eckert, N., and Naaim, M.:
416 Evaluation of slope stability with respect to snowpack spatial variability, *J. Geophys. Res.*, 2014.
417 doi: 10.1002/2014JF00319, 2014.
- 418 Gauthier, D. and Jamieson, B.: Evaluation of a prototype field test for fracture and failure
419 propagation propensity in weak snowpack layers, *Cold Reg. Sci. Technol.*, 51, 87-97, 2008a.
- 420 Gauthier, D. and Jamieson, B.: Fracture propagation propensity in relation to snow slab avalanche
421 release: Validating the Propagation Saw Test, *Geophys. Res. Lett.*, 35, L13501, 2008b.
- 422 Gauthier, D. and Jamieson, J. B.: Towards a field test for fracture propagation propensity in weak
423 snowpack layers, *J. Glaciol.*, 52, 164-168, 2006.
- 424 Habermann, M., Schweizer, J., and Jamieson, J. B.: Influence of snowpack layering on human-
425 triggered snow slab avalanche release, *Cold Reg. Sci. Technol.*, 54, 176-182, 2008.

426 Heierli, J.: Anticrack model for slab avalanche release, Ph.D. thesis, University of Karlsruhe, Karlsruhe,
427 Germany, 102 pp., 2008.

428 Jamieson, B., Haegeli, P., and Schweizer, J.: Field observations for estimating the local avalanche
429 danger in the Columbia Mountains of Canada, *Cold Reg. Sci. Technol.*, 58, 84-91, 2009.

430 Jamieson, J. B.: Avalanche prediction for persistent snow slabs. Ph.D. thesis, Department of Civil
431 Engineering, University of Calgary, Calgary AB, Canada, 258 pp., 1995.

432 Jamieson, J. B. and Johnston, C. D.: Refinements to the stability index for skier-triggered dry slab
433 avalanches, *Ann. Glaciol.*, 26, 296-302, 1998.

434 Jamieson, J.B. and Johnston, C.D.: Evaluation of the shear frame test for weak snowpack layers. *Ann.*
435 *Glaciol.*, 32, 59-68, 2001.

436 Johnson, J. B. and Schneebeli, M.: Characterizing the microstructural and micromechanical properties
437 of snow, *Cold Reg. Sci. Technol.*, 30, 91-100, 1999.

438 Lehning, M., Fierz, C., Brown, R. L., and Jamieson, J. B.: Modeling instability for the snow cover model
439 SNOWPACK, *Ann. Glaciol.*, 38, 331-338, 2004.

440 Löwe, H. and van Herwijnen, A.: A Poisson shot noise model for micro-penetration of snow, *Cold Reg.*
441 *Sci. Technol.*, 70, 62-70, 2012.

442 Mahajan, P. and Joshi, S.K.: Modeling of interfacial crack velocities in snow, *Cold Reg. Sci. Technol.*,
443 51(2-3), 98-111, 2008.

444 Marshall, H.-P. and Johnson, J. B.: Accurate inversion of high-resolution snow penetrometer signals
445 for microstructural and micromechanical properties, *J. Geophys. Res.*, 114, F04016, 2009.

446 McClung, D. M.: Dry snow slab quasi-brittle fracture initiation and verification from field tests, *J.*
447 *Geophys. Res.*, 114, F01022, doi:10.1029/2007JF000913, 2009.

448 McClung, D. M. and Schaerer, P.: *The Avalanche Handbook*, The Mountaineers Books, Seattle WA,
449 U.S.A., 2006.

450 McClung, D. M. and Schweizer, J.: Skier triggering, snow temperatures and the stability index for dry
451 slab avalanche initiation, *J. Glaciol.*, 45, 190-200, 1999.

452 Monti, F., Schweizer, J., and Gaume, J.: Deriving snow stability information from simulated snow
453 cover stratigraphy, *Proceedings ISSW 2014. International Snow Science Workshop, Banff,*
454 *Alberta, Canada, 29 September - 3 October 2014, 465-469, 2014.*

455 Perla, R.: Slab avalanche measurements, *Can. Geotech. J.*, 14(2), 206-213, 1977.

456 Perla, R., Beck, T. M. H., and Cheng, T. T.: The shear strength index of alpine snow, *Cold Reg. Sci.*
457 *Technol.*, 6, 11-20, 1982.

458 Pielmeier, C. and Marshall, H.-P.: Rutschblock-scale snowpack stability derived from multiple quality-
459 controlled SnowMicroPen measurements, *Cold Reg. Sci. Technol.*, 59, 178-184, 2009.

460 Podolskiy, E. A., Chambon, G., Naaim, M., and Gaume, J.: A review of finite-element modelling in
461 snow mechanics, *J. Glaciol.*, 59, 1189-1201, 2013.

462 Proksch, M., Löwe, H., and Schneebeli, M.: Density, specific surface area and correlation length of
463 snow measured by high-resolution penetrometry, *J. Geophys. Res.*, 120, doi:
464 10.1002/2014JF003266, 2015.

465 Reuter, B., Proksch, M., Loewe, H., van Herwijnen, A., and Schweizer, J.: On how to measure snow
466 mechanical properties relevant to slab avalanche release, *Proceedings ISSW 2013.*
467 *International Snow Science Workshop, Grenoble, France, 7-11 October 2013, 7-11, 2013.*

468 Reuter, B. and Schweizer, J.: The effect of surface warming on slab stiffness and the fracture behavior
469 of snow, *Cold Reg. Sci. Technol.*, 83-84, 30-36, 2012.

470 Roch, A.: Les déclenchements d'avalanches. In: *Symposium at Davos 1965 - Scientific Aspects of*
471 *Snow and Ice Avalanches*, IAHS Publication, 69, Int. Assoc. Hydrol. Sci., Wallingford, U.K., 1966.

472 Scapozza, C.: Entwicklung eines dichte- und temperaturabhängigen Stoffgesetzes zur Beschreibung
473 des visko-elastischen Verhaltens von Schnee, Ph.D. thesis, Institut für Geotechnik, ETH Zurich,
474 Zurich, Switzerland, 250 pp., 2004.

475 Schneebeli, M.: Numerical simulation of elastic stress in the microstructure of snow, *Ann. Glaciol.*, 38,
476 339-342, 2004.

477 Schneebeli, M. and Johnson, J. B.: A constant-speed penetrometer for high-resolution snow
478 stratigraphy, *Ann. Glaciol.*, 26, 107-111, 1998.

479 Schweizer, J.: The influence of the layered character of snow cover on the triggering of slab
480 avalanches, *Ann. Glaciol.*, 18, 193–198, 1993.

481 Schweizer, J.: The Rutschblock test - Procedure and application in Switzerland, *The Avalanche*
482 *Review*, 20, 1, 14-15, 2002.

483 Schweizer, J. and Jamieson, J. B.: Snowpack properties for snow profile analysis, *Cold Reg. Sci.*
484 *Technol.*, 37, 233-241, 2003.

485 Schweizer, J. and Jamieson, J. B.: Snowpack tests for assessing snow-slope instability, *Ann. Glaciol.*,
486 51, 187-194, 2010.

487 Schweizer, J. and Kronholm, K.: Snow cover spatial variability at multiple scales: Characteristics of a
488 layer of buried surface hoar, *Cold Reg. Sci. Technol.*, 47, 207-223, 2007.

489 Schweizer, J. and Reuter, B.: A new index combining weak layer and slab properties for snow
490 instability, *Nat. Hazards Earth Syst. Sci.*, 15, 109-118, 2015.

491 Schweizer, J., Bellaire, S., Fierz, C., Lehning, M., and Pielmeier, C.: Evaluating and improving the
492 stability predictions of the snow cover model SNOWPACK, *Cold Reg. Sci. Technol.*, 46, 52-59,
493 2006.

494 Schweizer, J., Jamieson, J. B., and Schneebeli, M.: Snow avalanche formation, *Rev. Geophys.*, 41,
495 1016, 2003.

496 Schweizer, J., Kronholm, K., Jamieson, J. B., and Birkeland, K. W.: Review of spatial variability of
497 snowpack properties and its importance for avalanche formation, *Cold Reg. Sci. Technol.*, 51,
498 253-272, 2008a.

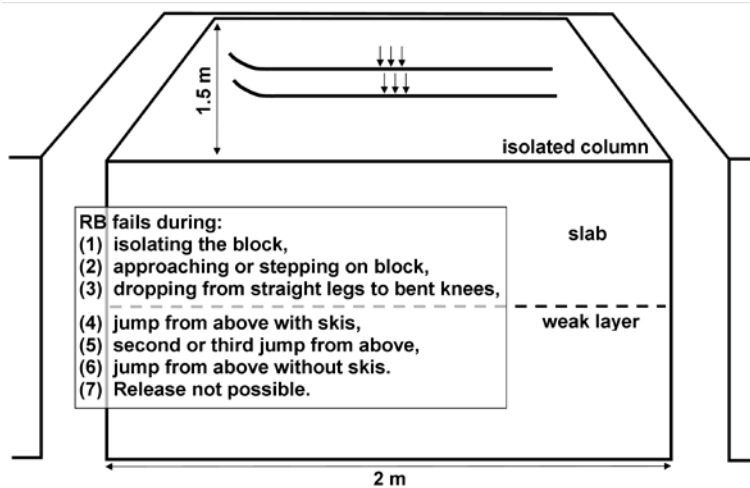
499 Schweizer, J., McCammon, I., and Jamieson, J. B.: Snowpack observations and fracture concepts for
500 skier-triggering of dry-snow slab avalanches, *Cold Reg. Sci. Technol.*, 51, 112-121, 2008b.

501 Schweizer, J., van Herwijnen, A., and Reuter, B.: Measurements of weak layer fracture energy, *Cold*
502 *Reg. Sci. Technol.*, 69, 139-144, 2011.

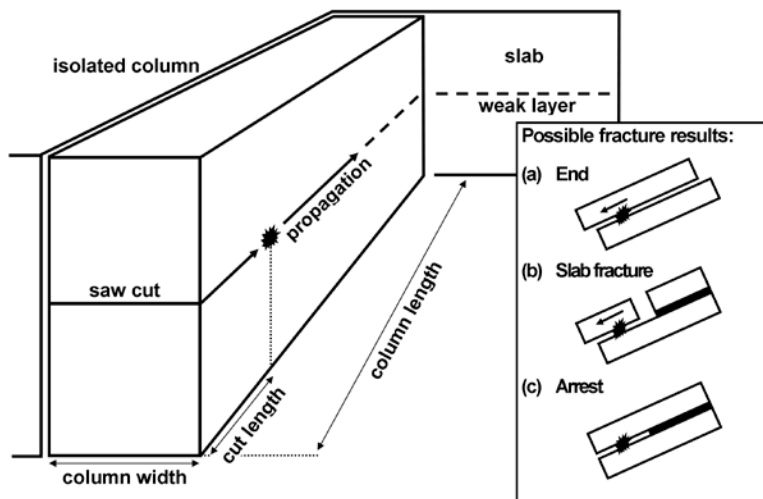
503 Sigrist, C. and Schweizer, J.: Critical energy release rates of weak snowpack layers determined in field
504 experiments, *Geophys. Res. Lett.*, 34, L03502, doi:03510.01029/02006GL028576, 2007.

505 van Herwijnen, A., Schweizer, J., and Heierli, J.: Measurement of the deformation field associated
506 with fracture propagation in weak snowpack layers, *J. Geophys. Res.*, 115, F03042,
507 doi:03010.01029/02009JF001515, 2010.

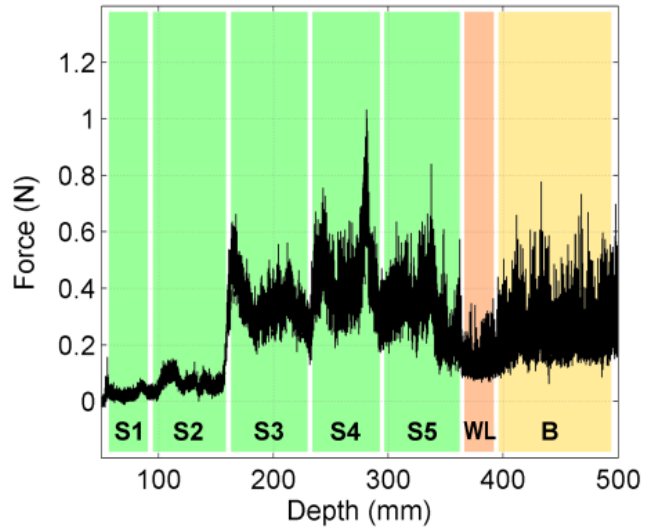
Figure Captions and Figures



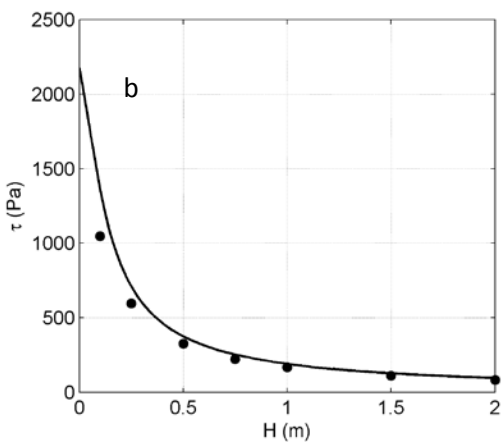
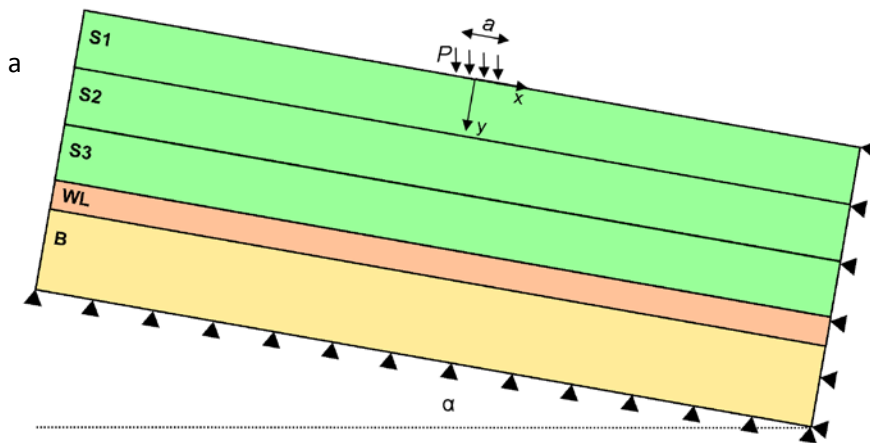
508 Figure 1: Sketch presenting the rutschblock (RB) test as it is seen looking upslope: After isolating a
 509 block of snow 2 m wide and 1.5 m upslope it is loaded progressively by a skier. The loading steps and
 510 scores are described in the inset. The release type was not considered here.



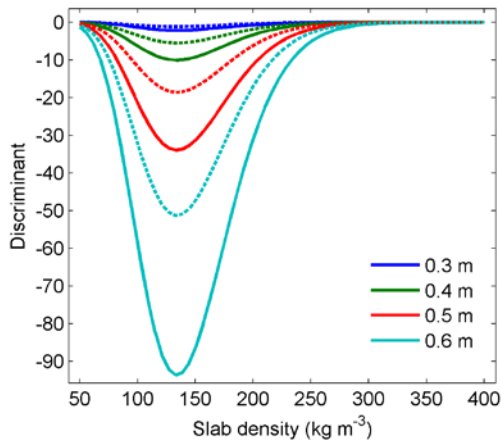
511
 512 Figure 2: Sketch presenting the propagation saw test (PST) as it is seen looking upslope: After
 513 isolating a column 30 cm wide and at least 1.2 m upslope, the weak layer is cut with a snow saw from
 514 its lower end continuing upslope. Possible fracture results are described in the inset. Here, we only
 515 consider tests where the fracture went to the end of the column (End).



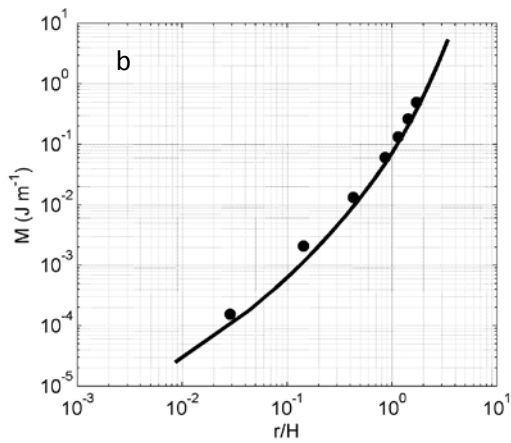
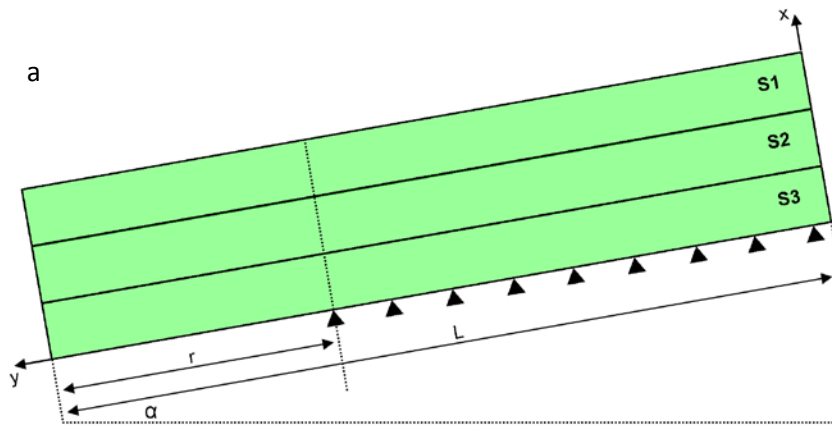
516 Figure 3: Penetration resistance (black) as measured with the SMP vs. snow depth. Slab layers (S1 to
 517 S5) shaded in light green, weak layer (W) shaded in light red, basal layer (B) shaded in light orange.
 518 50 mm of air signal cut off.



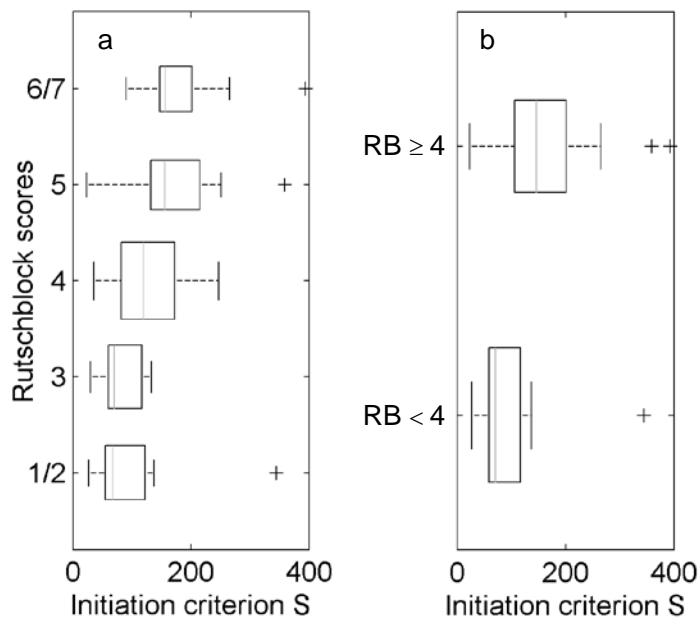
519 Figure 4: (a) FE model to simulate the maximum shear stress at the depth of the weak layer
 520 consisting of three slab layers (green), the weak layer (red) and a basal layer below (orange) inclined
 521 by the slope angle α . Triangles indicate fixed nodes. The applied strip load P is illustrated by black
 522 arrows pointing towards the snow surface. The axes of the coordinate system are indicated by
 523 arrows. (b) Maximum shear stress from FE simulations (dots) and from the analytical solution (line)
 524 for a uniform slab with density 200 kg m^{-3} and a slope angle of 38° versus slab thickness H .



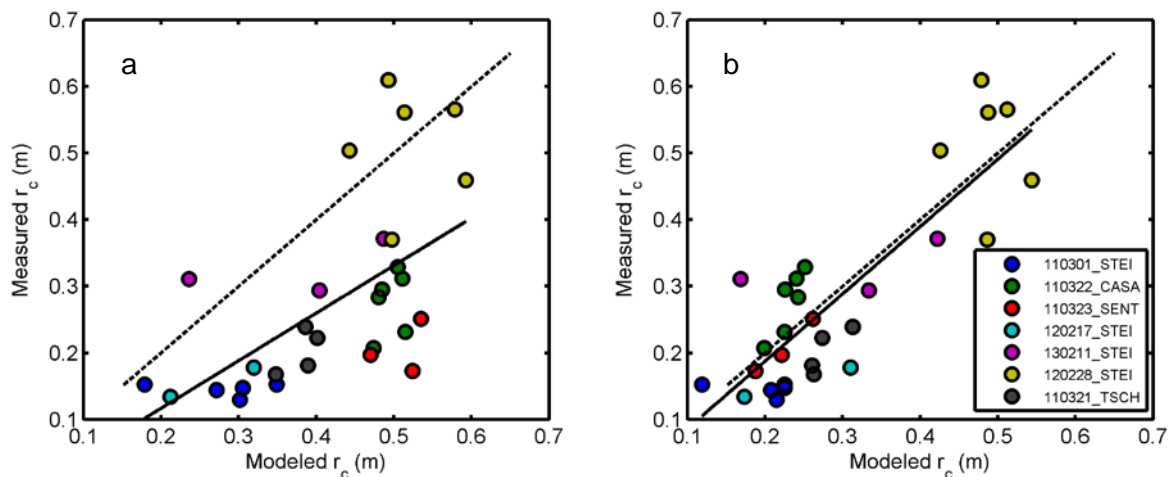
525 Figure 5: The polynomial's (Eq. 5) discriminant versus slab density for typical values of slab thickness
 526 (colors); different line styles indicate flat terrain (dashed) and a slope inclined by $\alpha = 38^\circ$ (solid lines).



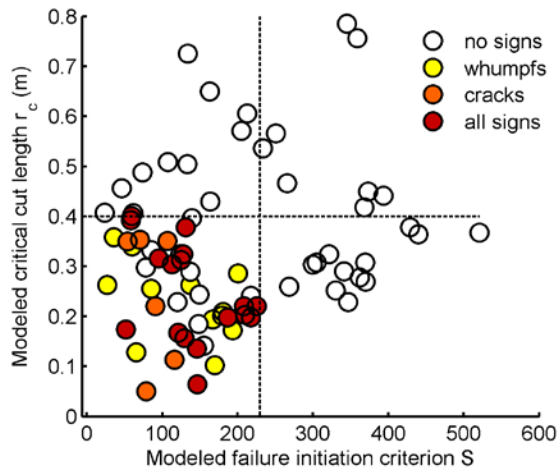
527 Figure 6: (a) The FE model to calculate the equivalent effective modulus contains as many slab layers
 528 as necessary to reflect the stratigraphy found in the SMP signal. Triangles indicate fixed nodes. The
 529 beam of length L is overhanging a crack of length r and is inclined by the slope angle α . (b)
 530 Mechanical energy M over the ratio of crack length and slab thickness (r/H) modeled with FE (dots)
 531 and calculated from the analytical solution (line) for a homogeneous slab with density 200 kg m^{-3} and
 532 a slope angle of 30° .



533 Figure 7: Modeled failure initiation criterion S (a) vs. RB score and (b) vs. RB stability classes: $RB < 4$
 534 ($N = 38$) and $RB \geq 4$ ($N = 26$). Boxes span the interquartile range from 1st to 3rd quartile with a
 535 horizontal line showing the median (grey line). Widths of the boxes correspond to the number of
 536 cases. Whiskers extend to the most extreme data points not considered outliers (crosses) within 1.5
 537 times the interquartile range above the 3rd and below the 1st quartile.



538 Figure 8: Critical crack lengths r_c predicted from Eq. 7 are contrasted with critical crack lengths
 539 measured in the field ($N = 31$). Experiments grouped by date and location with colors. Solid line
 540 shows linear regression, dashed line indicates the 1:1 line. (a) Slab stratigraphy neglected (average
 541 density, average effective modulus). (b) Density and effective modulus of each snow layer taken into
 542 account by FE simulation.



543 Figure 9: Type and presence of signs of instability against failure initiation criterion S and critical crack
 544 length r_c , both modeled, for datasets A and B, if reported ($N = 77$). Colors indicate type of observed
 545 signs of instability: whumpfs, shooting cracks with or without whumpfs (cracks) or all signs
 546 (whumpfs, cracks and recent avalanches observed). Open circles indicate that no signs of instability
 547 were reported explicitly (no signs). Dashed lines represent split values dividing the plot into four
 548 quadrants as found with a classification tree.